LANGMUIR
Article
Cite This: Langmuir 2018, 34, 6806−6813
pubs.acs.org/Langmuir

Synthesis of Transparent Aqueous ZrO_2 Nanodispersion with a Controllable Crystalline Phase without Modification for a High-Refractive-Index Nanocomposite Film

Yi Xia,[†,‡] Cong Zhang,[‡] Jie-Xin Wang,*[,†,‡] Dan Wang,[†] Xiao-Fei Zeng,[†] and Jian-Feng Chen[†,‡]

[†]Beijing Advanced Innovation Center for Soft Matter Science and Engineering, State Key Laboratory of Organic−Inorganic Composites, and [‡]Research Center of the Ministry of Education for High Gravity Engineering and Technology, Beijing University of Chemical Technology, Beijing 100029, PR China

ABSTRACT: The controllable synthesis of metal oxide nanoparticles is of fundamental and technological interest. In this article, highly transparent aqueous nanodispersion of ZrO_2 with controllable crystalline phase, high concentration, and long-term stability was facilely prepared without any modification via the reaction of inexpensive inorganic zirconium salt and sodium hydroxide in water under an acid surrounding, combined with hydrothermal treatment. The as-prepared transparent nanodispersion had an average particle size of 7 nm, a high stability of 18 months, and a high solid content of 35 wt %. ZrO_2 nanocrystals could be readily dispersed in many solvents with high polarity including ethanol, dimethyl sulfoxide, acetic acid, ethylene glycol, and *N*,*N*-dimethylformamide, forming stable transparent nanodispersions. Furthermore, highly transparent polyvinyl alcohol/ZrO_2 nanocomposite films with high refractive index were successfully prepared with a simple solution mixing route. The refractive index could be tuned from 1.528 to 1.754 (@ 589 nm) by changing the mass fraction (0−80 wt %) of ZrO_2 in transparent nanocomposite films.

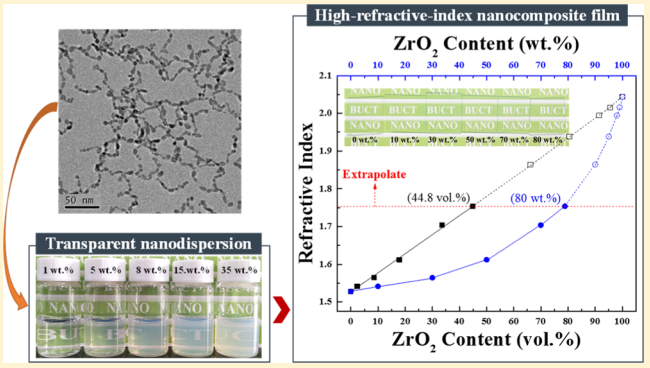

1. INTRODUCTION

Recently, functional polymer−inorganic hybrid materials have attracted a great deal of attention owing to the outstanding combinations of mechanical,[1,2] thermal,[3] magnetic,[4] surface,[5,6] optical,[7,8] electronic,[9] antiswelling,[10] biomedical,[11−13] and optoelectronic[14,15] properties when compared with individual polymer or inorganic components. In particular, optically transparent nanocomposite materials with high refractive index, having the potential applications in antireflection films,[16−18] optical waveguides,[19] plastic optical fibers,[20] photonic crystals,[21] lenses,[22] and whispering gallery mode,[23] have been extensively studied. In these cases, the inorganic domains must be controlled to be below one-tenth of the wavelength of visible light (400−800 nm) for reducing scattering loss and maintaining the optical transparency.[24] Ideally, the inorganic particles should have a diameter below 10 nm because the presence of even a small percentage of larger particles or aggregates may result in excessive light scattering in the visible region, causing haze or even turbidity.[25] In addition, it is also desired to achieve homogeneous dispersion and excellent stability of nanoparticles at a high solid content in the polymer matrix for such an optical application.

So far, some semiconductor nanoparticles of metal sulfides such as PbS,[26] FeS,[27] ZnS,[28−30] and metal oxides such as TiO_2,[31,32] ZrO_2,[33,34] and ZnO[35] owing to their high refractive index are usually introduced into the polymer matrix to prepare nanocomposites with high refractive index. However, sulfur-containing raw materials such as Na_2S and H_2S to prepare PbS, ZnS, and FeS suffer from pollution and storage problems. TiO_2 and ZnO have photocatalytic properties, resulting in the obviously reduced optical transparency of hybrid films at a wavelength of around 400 nm owing to the low band gap of TiO_2 (3.2 eV)[9] and ZnO (3.37 eV)[36] and the possibly accelerated decomposition of polymer matrix. Recently, ZrO_2 nanocrystals have been an ideal building block for high-refractive-index nanocomposites because they offer several advantages such as chemical inertness, excellent thermal stability, high hardness,[37,38] and excellent optical properties, such as Abbe number and transparency on a broad spectral range because of the large band gap of ZrO_2 in the range of 5.0−5.85 eV.[24] Presently, some methods have been developed for the synthesis of ZrO_2 nanocrystals, including sol−gel method,[39] solvothermal method,[40,41] two-phase method,[42] and nonaqueous method.[7,38] However, there are still several challenges. First, the commonly used synthetic methods usually employ expensive and unstable organic alkoxide precursors, such as zirconium(IV) propoxide and zirconium(IV) butoxide, which are sensitive to moisture, air, and light.[7,43,44] Second, the

Received: January 17, 2018
Revised: April 10, 2018
Published: May 17, 2018

DOI: 10.1021/acs.langmuir.8b00160
Langmuir 2018, 34, 6806−6813

as-obtained nanocrystals, covered with long alkyl chain fatty acids or amines, usually have hydrophobic surface properties, thereby limiting their wide applications.[45] Third, ZrO_2 exists in three polymorphs: the monoclinic (M-ZrO_2), tetragonal (T-ZrO_2), and cubic (C-ZrO_2) phases. However, it is hard to realize the controllable preparation of pure-phase tetragonal and monoclinic nanocrystals in the size of about 10 nm.[42] Therefore, it is urgent to develop a facile way to prepare aqueous dispersion of ZrO_2 nanocrystals with controllable crystalline phase, high solid content, and stability.

In this work, a novel and cost-effective route was presented to prepare transparent aqueous zirconia nanodispersions with controllable crystalline phase without any surface modification. In this case, high-yield zirconia nanocrystals were synthesized via the reaction of inexpensive inorganic zirconium salt and sodium hydroxide in an acid aqueous surrounding, followed by the regulated hydrothermal process. The as-prepared zirconia nanocrystals could be readily dispersed in many solvents with high polarity, forming long-term stable and transparent nanodispersions with high solid content. Furthermore, highly transparent hydrophilic polyvinyl alcohol (PVA)/ZrO_2 nanocomposite films with high refractive index were prepared by a simple solution mixing approach. The related optical properties and refractive index were also investigated.

2. EXPERIMENTAL SECTION

2.1. Chemicals. Zirconium oxychloride octahydrate ($ZrOCl_2 \cdot 8H_2O$), sodium hydroxide (NaOH), ethanol (ET), ethylene glycol (EG), and *N*,*N*-dimethylformamide (DMF) were purchased from Beijing Chemical Reagent Co. PVA with a polymerization degree of 1750 ± 50 and a saponification degree of 98−99% was obtained from Tianjin Fuchen Chemical Reagents Factory. All of the chemical reagents were analytically pure and used without further purification. Deionized water was purified by a water purification system (RO-DI plus, Hitech, PRC).

2.2. Preparation of Transparent Aqueous ZrO_2 Nanodispersions. The whole synthesis procedure consisted of two steps (Scheme 1): first, controlled growth of −Zr−O−Zr− networks from

Scheme 1. Proposed Formation Mechanism of ZrO_2 Nanocrystals

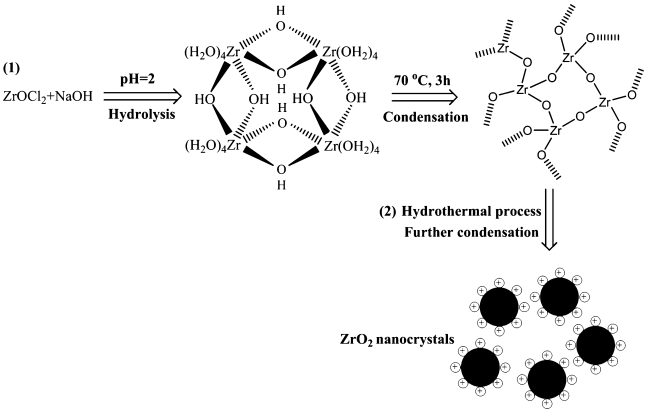

hydrolysis[46] and condensation reaction of $ZrOCl_2$ in the acid environment of pH = 2, forming transparent zirconium hydroxide precursor and second, further condensation of −Zr−O−Zr− networks by a hydrothermal method, eliminating the need for any subsequent calcination step to crystallization.

Typically, 2.0946 g (6.5 mmol) of $ZrOCl_2 \cdot 8H_2O$ was dissolved in 65 mL of deionized water at 25 °C under vigorous stirring. An aqueous solution (38 mL) containing 0.19 g (4.75 mmol) of NaOH was then added dropwise into the above $ZrOCl_2$ aqueous solution. The final pH value of the mixture was 2.0. In addition, the mixture was further stirred at 70 °C for 3 h. Subsequently, the as-obtained zirconium hydroxide precursor was washed thoroughly with deionized water by a dialysis method. Finally, the precursor was transferred into a 200 mL Teflon-lined stainless steel autoclave and heat-treated at 170 °C for 10 h to form transparent aqueous dispersions of ZrO_2 nanocrystals with coexistent monoclinic and tetragonal phases.

Transparent dispersions of pure M-ZrO_2 nanocrystals were achieved only by increasing the hydrothermal temperature to 230 °C. In addition, transparent dispersions of pure T-ZrO_2 nanocrystals were prepared by replacing two-third of water with EG and increasing the hydrothermal temperature to 240 °C. Other processes were the same as the above description.

2.3. Preparation of a Transparent PVA/ZrO_2 Nanocomposite Film. Transparent PVA/ZrO_2 nanocomposite films with high refractive index were fabricated by a facile solution mixing method. Typically, PVA was first dissolved in the deionized water at 90 °C under vigorous stirring for 1 h to obtain a homogeneous solution. Subsequently, transparent ZrO_2 nanodispersions with different solid contents were added into the above PVA solution. The formed mixture was sonicated for 10 min until a homogeneous and transparent solution was obtained. Finally, the above PVA/ZrO_2 solution was coated on a glass sheet or silicon wafer by a spin-coating process to obtain PVA/ZrO_2 nanocomposite films. The films were kept at a room temperature for 24 h to ensure the solvent fully evaporated. For a comparison, ZrO_2 nanopowder dried from ZrO_2 nanodispersion was also used to prepare ZrO_2/PVA nanocomposite films with the same method.

2.4. Characterization. The size and the morphology of ZrO_2 nanocrystals were examined with a transmission electron microscope (TEM, JEM-2100, JEOL, Japan) operating at an accelerating voltage of 120 KV. The surface potential of ZrO_2 nanocrystals was measured with a particle size and zeta potential analyzer (Nano-ZS90, Malvern, Britain). The crystalline structure of ZrO_2 nanocrystals was performed by an X-ray diffractometer (XRD-6000, Shimadzu, Japan) equipped with Cu Kα radiation, an accelerating voltage of 40 kV and a current of 40 mA. The scanning range was 10°−80°, and the scanning rate was 5°/min with a step size of 0.02°. Raman spectroscopy (HORIBA Jobin Yvon LabRAM ARAMIS) was recorded at a room temperature with 532 nm excitation line of a diode-pumped solid-state laser in the wavenumber range of 100−700 cm^{-1}. The Fourier transform infrared (FTIR) spectrum was recorded with a Nicolet 6700 spectrometer (Nicolet Instrument Co., USA) in the range of 400−4000 cm^{-1}. The transparency of ZrO_2/PVA nanocomposite films was characterized by a UV−vis spectrometer (UV-2501, Shimadzu, Japan) in the range from 200 to 800 nm. The refractive index of the films was tested by an ellipsometer (UVSEL, HORIBA, France) in the wavelength range of 260−800 nm.

3. RESULTS AND DISCUSSION

Figure 1 displays representative TEM images, the corresponding particle size distribution, the digital photograph, and the FTIR spectrum of the as-prepared aqueous dispersion of ZrO_2 nanocrystals. It could be clearly seen that the near-spherical ZrO_2 nanoparticles had a narrow size distribution with an average diameter of 7 nm. Despite no surface modification, the aqueous dispersion of ZrO_2 nanocrystals still had high transparency and could maintain a long-term stability for over 18 months without precipitation. No use of surface modifiers was beneficial to optical high-refractive-index applications without the interference from the organic modification layer. Previously, Chung et al.[47] reported that the ZrO_2 nanocrystals modified by butyric acid and silane had an obviously decreased refractive index of 1.762 (@589 nm), which was much lower than an intrinsic refractive index of ~2.2 (@589 nm) of ZrO_2 nanocrystals without modification. In this study, the possible formation reason of stable aqueous dispersion of ZrO_2

DOI: 10.1021/acs.langmuir.8b00160
Langmuir 2018, 34, 6806−6813

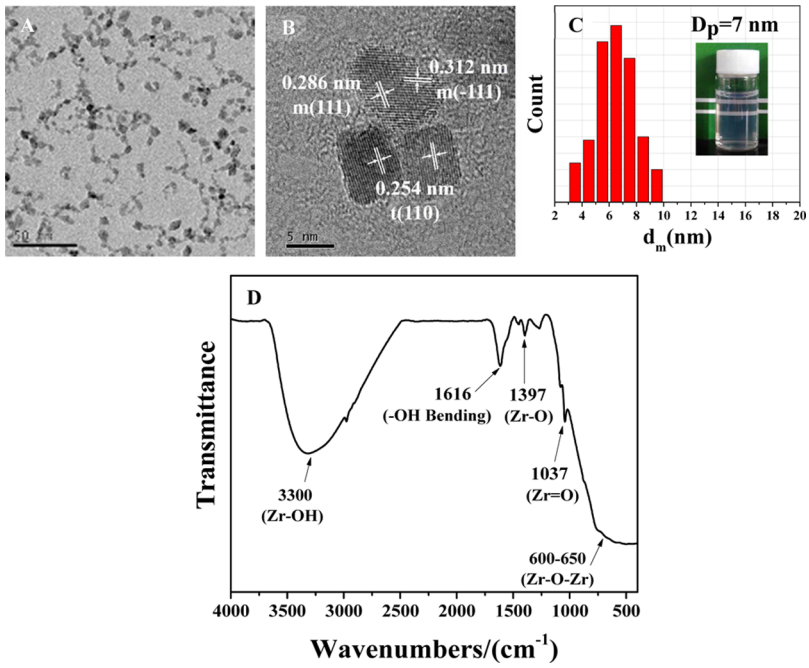

Figure 1. TEM image (A), high-resolution TEM (HRTEM) image (B), and particle size distribution (C) (the inset is a digital photograph of ZrO_2 nanodispersions with a solid content of 1 wt %) and FTIR spectrum of ZrO_2 nanocrystals.

nanocrystals without modification is that zirconium hydroxide precursor is created in a homogeneous acid environment without any precipitate. Oxygen vacancy is thus formed in the crystal lattice, thereby leading to the generation of ZrO_2 nanocrystals with high positive charge in the condensation process, as shown in Scheme 1. The surface potential of as-prepared aqueous dispersion of ZrO_2 nanocrystals was high enough (+53.7 mV) so that the Coulomb force could prevent particles from agglomeration and form a stable dispersion. In addition, the clear lattice image of isolated particles indicated the high crystallinity of the as-synthesized nanocrystals. The lattice spacings of 0.286 and 0.312 nm corresponded to (111) and (−111) planes of the M-ZrO_2 structure, respectively, whereas the lattice spacing of 0.254 nm corresponded to the (110) plane of the T-ZrO_2 structure. The results demonstrated that the obtained ZrO_2 nanocrystals existed in both monoclinic and tetragonal phases. To analyze the composition of ZrO_2 nanocrystals, FTIR was further performed. The result indicated that the broad band around 3300 cm^{-1} resulted from the OH groups on the surface of ZrO_2 nanoparticles.[24] The band centered upon 1616 cm^{-1} was related to the coordinated water because of the −OH bending mode of molecular water.[48] The multiple peaks around 1397 cm^{-1} could be assigned to the coordinatively unsaturated O^{-2}–Zr^{4+} pairs.[48] The weak band around 1037 cm^{-1} was ascribed to zirconyl group Zr═O. The strong peak in the range of 400−700 cm^{-1} was the Zr−O−Zr vibration mode.[40]

Figure 2 shows the XRD pattern and Raman spectrum of the as-prepared ZrO_2 nanocrystals. As shown in Figure 2A, the diffraction peaks at 24.16°, 24.63°, 28.34°, and 31.48° belonged to monoclinic phase ZrO_2 according to PDF 80-0966. However, it is hard for the diffraction peaks at 30°, 35°, 50°, and 60° to distinguish cubic and tetragonal phases of ZrO_2 according to PDF 88-1007 and PDF 49-1642. The results indicated that the as-prepared ZrO_2 nanocrystals were a mixture of monoclinic and tetragonal (or cubic) phases, and XRD analysis was insensitive to identifying the tetragonal and

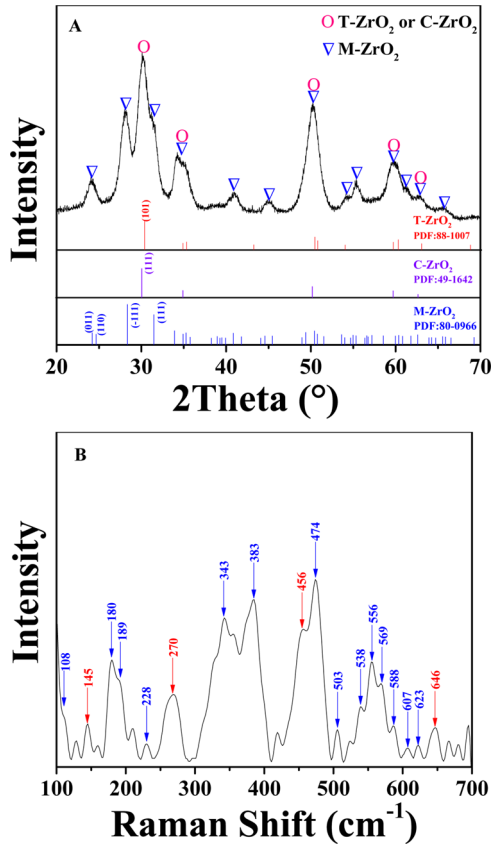

Figure 2. XRD pattern (A) and Raman spectrum (B) of ZrO_2 nanocrystals.

cubic phases of ZrO_2. To make a distinction between tetragonal and cubic phases, Raman spectroscopy was used as an additional technique (Figure 2B). There were 14 out of 18 theoretically predicted monoclinic bands.[49] The strong peaks at

DOI: 10.1021/acs.langmuir.8b00160
Langmuir 2018, 34, 6806−6813

145, 270, 456, and 646 cm^{-1} were assigned to the tetragonal phase because cubic ZrO_2 had a broad band in the range of 530−670 cm^{-1}.[50] Therefore, Raman results completely proved that the as-obtained ZrO_2 nanocrystals were a mixture of coexisting monoclinic and tetragonal phases, which was in good accordance with the above TEM data.

To obtain transparent dispersions of pure monoclinic and tetragonal phase ZrO_2 nanocrystals, hydrothermal temperature and medium were altered. Hydrothermal temperature was first changed at the same hydrothermal medium. Figure 3 shows

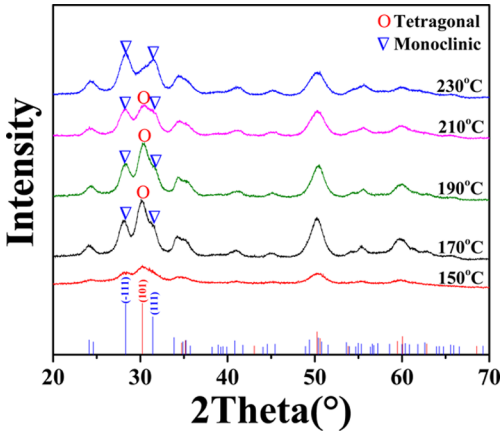

Figure 3. XRD patterns of ZrO_2 nanocrystals prepared at different hydrothermal temperatures.

XRD patterns of ZrO_2 nanocrystals prepared at varying hydrothermal temperatures in the range of 150−230 °C for 10 h. Clearly, decreasing the hydrothermal temperature to 150 °C caused the simultaneous crystallinity weakening of monoclinic and tetragonal phases of ZrO_2 nanocrystals. Upon increasing the hydrothermal temperature from 170 to 230 °C, there was a gradual increase of the intensity of diffraction peaks at 28.34° and 31.48° belonging to the monoclinic (−111) and (111) lines, whilst the (101) line at 30.27° of tetragonal ZrO_2 gradually disappeared between the two monoclinic lines. In order to quantitatively elucidate ZrO_2 polymorph, Table 1 gives

Table 1. Mass Fraction of Monoclinic Phase of the Products Obtained at Different Hydrothermal Temperatures

hydrothermal temperature (°C)	M-ZrO_2/wt %
150	0.284
170	0.551
190	0.608
210	0.713
230	1.000

the mass fraction of monoclinic phase of ZrO_2 nanocrystals obtained at the corresponding hydrothermal temperatures, which is calculated by Jade 6. With the increased hydrothermal temperature from 150 to 230 °C, the mass fraction of M-ZrO_2 phase obviously increased from 0.284 to 1. At this time, the mixed crystal phase was successfully converted to the pure monoclinic phase at 230 °C, indicating that higher hydrothermal temperature favored the formation of M-ZrO_2 phase. Figure 4 shows typical TEM images and the corresponding digital photograph of aqueous dispersion of pure M-ZrO_2 nanocrystals. Clear lattice fringes with a lattice spacing of 0.316 nm were obviously observed, corresponding to the

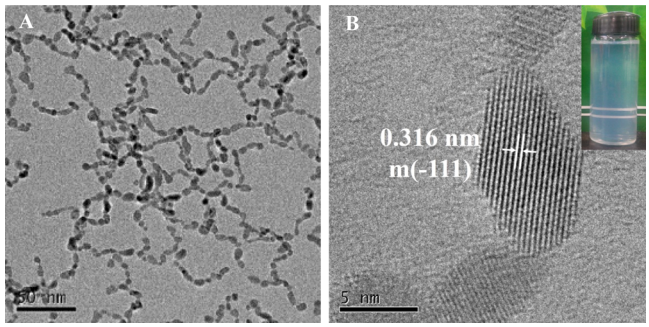

Figure 4. TEM image (A) and HRTEM image (B) of pure M-ZrO_2 nanocrystals (the inset is a digital photograph of M-ZrO_2 nanodispersions with a solid content of 1 wt %).

(−111) plane of M-ZrO_2 nanocrystals. As compared to the counterpart with mixed crystal phases, aqueous dispersion of pure M-ZrO_2 nanocrystals had chainlike particles with an almost unchanged size and a very slightly decreased transparency, but it still possessed an excellent stability.

To obtain pure tetragonal phase ZrO_2 nanocrystals, the choice of hydrothermal medium is crucial. Li et al.[41] reported that pure M-ZrO_2 and T-ZrO_2 nanocrystals were obtained in water and methanol, respectively. In our work, water as a hydrothermal medium was partially replaced with EG. Figure 5

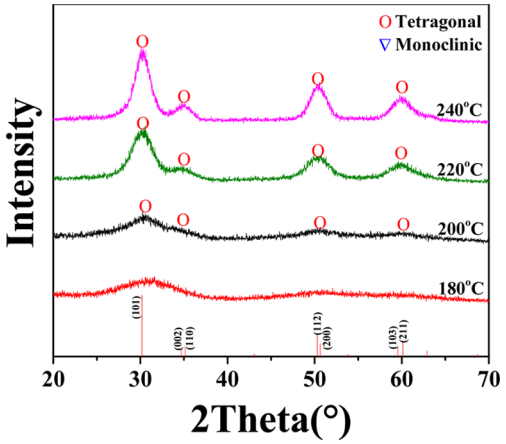

Figure 5. XRD patterns of ZrO_2 nanocrystals prepared in the water−EG mixed solvent with a volume ratio of 1:2 as a hydrothermal medium at different hydrothermal temperatures.

displays XRD patterns of ZrO_2 nanocrystals prepared in the water−EG mixed solvent with a volume ratio of 1:2 as a hydrothermal medium at different hydrothermal temperatures in the range of 180−240 °C for 10 h. With the increase of hydrothermal temperature to over 220 °C, there were strong diffraction peaks ascribed to pure tetragonal phase. Figure 6 shows TEM images and the corresponding digital photograph of the as-obtained dispersion of pure T-ZrO_2 nanocrystals. The transparent nanodispersion had a slightly increased particle aggregation possibly owing to the change of hydrothermal medium and higher hydrothermal temperature. In addition, there were clear lattice fringes with the lattice spacing of 0.299 nm, corresponding to the (101) plane of T-ZrO_2 nanocrystals. Interestingly, it is hard for other volume ratios of water−EG to achieve transparent dispersion of pure T-ZrO_2 nanocrystals. The related formation mechanism still needs to be further investigated.

DOI: 10.1021/acs.langmuir.8b00160
Langmuir 2018, 34, 6806−6813

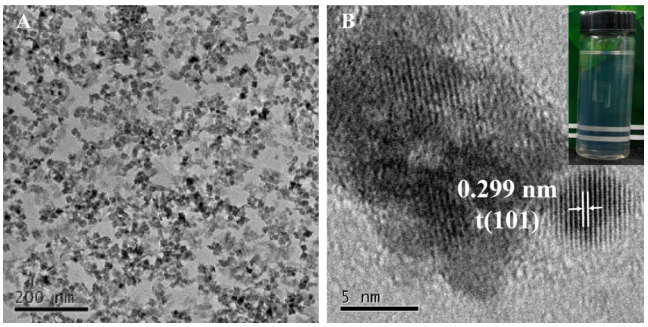

Figure 6. TEM image (A) and HRTEM image (B) of pure T-ZrO_2 nanocrystals (the inset is a digital photograph of T-ZrO_2 nanodispersions with a solid content of 1 wt %).

Figure 7 gives the digital photographs of aqueous dispersions of ZrO_2 nanocrystals with different solid contents, as well as

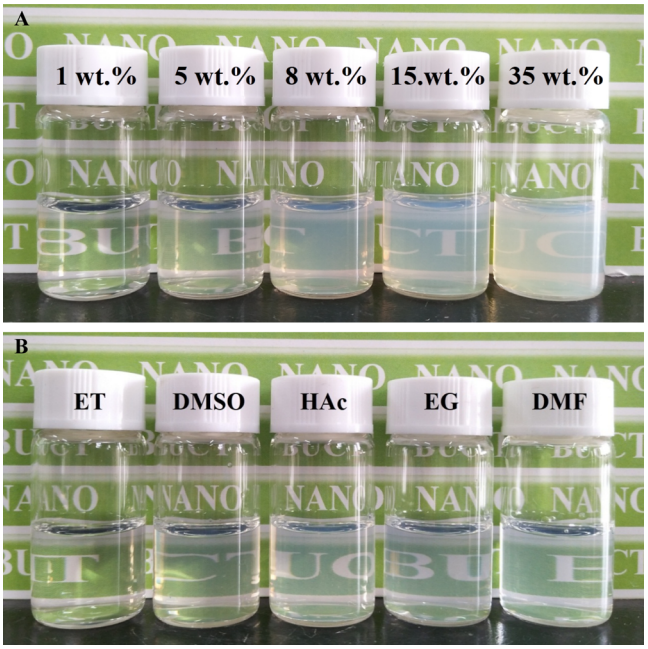

Figure 7. Digital photographs of aqueous ZrO_2 nanodispersions with different solid contents, and ZrO_2 nanodispersions with different dispersion media and the same solid content of 1 wt %.

ET, dimethyl sulfoxide (DMSO), acetic acid (HAc), EG, and DMF dispersions of ZrO_2 nanocrystals with a solid content of 1 wt %. Obviously, when the solid content was below 5%, clear and highly transparent ZrO_2 nanodispersion was visually identical to water. In addition, the transparency of ZrO_2 nanodispersions only slightly decreased with the increased ZrO_2 solid content from 5 to 15 wt %. ZrO_2 nanodispersions still maintained a good transparency when the solid content reached as high as 35 wt %, which was beneficial to optical high-refractive-index nanocomposite applications. Furthermore, the as-prepared ZrO_2 nanocrystals could be readily dispersed in many solvents with high polarity including ET, DMSO, HAc, EG, and DMF, forming long-term stable and transparent nanodispersions.

Figure 8 shows the digital photographs, the optical transmittance, and the refractive index of PVA/ZrO_2 nanocomposite films with different ZrO_2 contents prepared with transparent ZrO_2 nanodispersions and ZrO_2 nanopowders. The

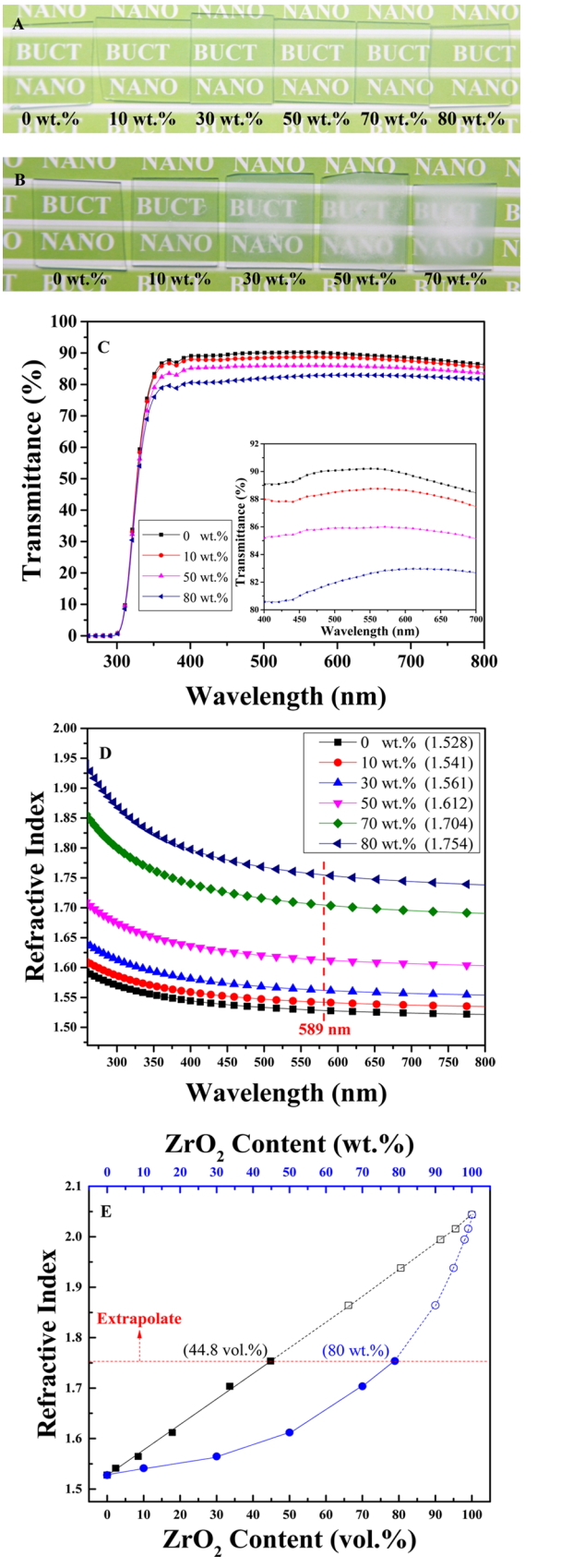

Figure 8. Digital photographs (A,B), the optical transmittance (C), and the refractive index (D,E) of PVA/ZrO_2 nanocomposite films with different ZrO_2 contents prepared from transparent ZrO_2 nanodispersions (A) and ZrO_2 nanopowders (B).

DOI: 10.1021/acs.langmuir.8b00160
Langmuir 2018, 34, 6806−6813

Table 2. Comparison of Reported Different Transparent Polymer/ZrO_2 Nanocomposites with High Refractive Index

refs	ZrO_2 diameter/nm	polymer matrix	ZrO_2 content in nanocomposites	refractive index
24	6	polyimide	0−50 wt %	1.632−1.804 (@633 nm)
21	6.1	PEO	0−70 wt % (42 vol %)	1.45−1.70 (@589 nm)
51	5.5	PVT	0−61.5 wt % (21.5 vol %)	1.533−1.649 (@633 nm)
47	6.6	oligosiloxane	0−51.7 wt % (37.7 vol %)	1.541−1.625 (@589 nm)
this work	7	PVA	0−80 wt % (44.8 vol %)	1.528−1.754 (@589 nm)

nanocomposite films from transparent ZrO_2 nanodispersions exhibited an excellent optical transparency (Figure 8A). With the increase of ZrO_2 content from 0 to 80 wt % in the nanocomposite film, the visible light transmittance in the range of 400−800 nm had only a slight decrease. The nanocomposite film had still an enough high transmittance of over 80% even when the ZrO_2 content was up to as high as 80 wt % (Figure 8C). In contrast, the corresponding nanocomposite films containing ZrO_2 nanopowders were transparent only at a ZrO_2 content of <10 wt %. However, it could be clearly observed that the films gradually became translucent and then opaque with the increased ZrO_2 powder content from 10 to 70 wt % (Figure 8B). Figure 8D shows the refractive index dispersion of the obtained films with different ZrO_2 solid contents in the range of 260−800 nm. Figure 8E displays the refractive index of the obtained films with different ZrO_2 volume contents and the corresponding weight contents at a wavelength of 589 nm. Obviously, the refractive index of PVA/ZrO_2 nanocomposite films (n_{PVA/ZrO_2}) increased linearly (R^2 = 0.9973) with the increased ZrO_2 volume fraction (φ_{ZrO_2}) from 0 to 44.8%, which followed the following equation

$$n_{PVA/ZrO_2} = 0.516\varphi_{ZrO_2} + 1.526$$

This is consistent with the effective medium theory of polymer nanocomposites.[51−53] The highest refractive index could reach 1.754 by increasing the corresponding mass fraction of ZrO_2 to 80%. By extrapolation, the refractive index of >2.0 could be theoretically achieved at a solid content of >98% in this system. However, it is very difficult to obtain higher refractive index by further increasing the content of ZrO_2 nanoparticles in this nanocomposite film. Table 2 gives the comparison of reported different transparent polymer/ZrO_2 nanocomposites with high refractive index. Clearly, with the similar particle size of about 6 nm, the highest ZrO_2 filling amount of 80 wt % in transparent polymer matrix was realized in this work, thereby demonstrating the great potential of ZrO_2 nanodispersion with high transparency, high solid content, and stability by this route in optical applications.

4. CONCLUSIONS

Highly transparent aqueous dispersions of ZrO_2 nanocrystals with tunable crystalline phase were prepared via the reaction of inexpensive $ZrOCl_2$ and NaOH in water under an acid surrounding, combined with hydrothermal treatment. The as-prepared ZrO_2 nanodispersions had an average particle size of 7 nm, a high solid content of 35 wt %, and an excellent stability of over 18 months. Furthermore, highly transparent PVA/ZrO_2 nanocomposite films with high refractive index were fabricated using a simple solution mixing method by adding transparent dispersions of ZrO_2 nanocrystals with high solid content into PVA solution. The refractive index could be altered in the range of 1.528−1.754 (@589 nm) by changing the mass fraction (0−80 wt %) of ZrO_2 nanocrystals in transparent nanocomposite films. It could be envisioned that such highly transparent organic−inorganic nanocomposites with high refractive index would be promising for various optical applications, including antireflection coatings, ophthalmic lenses, prisms, optical waveguides, nonlinear optical materials, adhesives for optical components, and so forth.

AUTHOR INFORMATION

Corresponding Author

*E-mail: wangjx@mail.buct.edu.cn. Phone: +86-10-64449453. Fax: +86-10-64423474.

ORCID

Jie-Xin Wang: 0000-0003-0459-1621

Dan Wang: 0000-0002-3515-4590

Xiao-Fei Zeng: 0000-0001-9010-0088

Notes

The authors declare no competing financial interest.

ACKNOWLEDGMENTS

This work was financially supported by National Key Research and Development Program of China (2016YFA0201701/2016YFA0201700), National Natural Science Foundation of China (21622601 and 21576022), and Guangdong Provincial Applied Science and Technology Research and Development Project (2015B090927001).

REFERENCES

(1) Schubert, U.; Völkel, T.; Moszner, N. Mechanical Properties of an Inorganic-Organic Hybrid Polymer Cross-Linked by the Cluster Zr_4O_2(methacrylate)$_{12}$. *Chem. Mater.* **2001**, *13*, 3811−3812.

(2) Podsiadlo, P.; Kaushik, A. K.; Arruda, E. M.; Waas, A. M.; Shim, B. S.; Xu, J.; Nandivada, H.; Pumplin, B. G.; Lahann, J.; Ramamoorthy, A. Ultrastrong and Stiff Layered Polymer Nanocomposites. *Science* **2007**, *318*, 80−83.

(3) Cho, H.-B.; Tokoi, Y.; Tanaka, S.; Suematsu, H.; Suzuki, T.; Jiang, W.; Niihara, K.; Nakayama, T. Modification of BN Nanosheets and Their Thermal Conducting Properties in Nanocomposite Film with Polysiloxane According to the Orientation of BN. *Compos. Sci. Technol.* **2011**, *71*, 1046−1052.

(4) Arai, T.; Sato, T.; Kanoh, H.; Kaneko, K.; Oguma, K.; Yanagisawa, A. Organic-Inorganic Hybrid Polymer-Encapsulated Magnetic Nanobead Catalysts. *Chem.—Eur. J.* **2010**, *14*, 882−885.

(5) Deshpande, P. A.; Polisetti, S.; Madras, G.; Jyothi, D.; Chandrasekaran, S. Dispersed ZrO_2 Nanoparticles in MCM-48 with High Adsorption Activity. *AIChE J.* **2012**, *58*, 2987−2996.

(6) Zhang, G.; Li, J.; Ji, S. Self-assembly of Novel Architectural Nanohybrid Multilayers and Their Selective Separation of Solvent-Water Mixtures. *AIChE J.* **2012**, *58*, 1456−1464.

(7) Garnweitner, G.; Goldenberg, L. M.; Sakhno, O. V.; Antonietti, M.; Niederberger, M.; Stumpe, J. Large-Scale Synthesis of Organophilic Zirconia Nanoparticles and Their Application in Organic-Inorganic Nanocomposites for Efficient Volume Holography. *Small* **2007**, *3*, 1626−1632.

(8) Seeni, R. Z.; Yu, X.; Chang, H.; Chen, P.; Liu, L.; Xu, C. Iron-Oxide Nanoparticles Powered Micro Optical Coherence Tomography for in Situ Imaging the Penetration and Swelling of Polymeric

DOI: 10.1021/acs.langmuir.8b00160
Langmuir 2018, 34, 6806−6813

Microneedles in Skin. *ACS Appl. Mater. Interfaces* **2017**, *9*, 20340−20347.
(9) Zeng, Q.; Zhang, X.; Feng, X.; Lu, S.; Chen, Z.; Yong, X.; Redfern, S. A. T.; Wei, H.; Wang, H.; Shen, H. Polymer-Passivated Inorganic Cesium Lead Mixed-Halide Perovskites for Stable and Efficient Solar Cells with High Open-Circuit Voltage over 1.3 V. *Adv. Mater.* **2018**, *30*, 1705393.
(10) Li, Y.; Jia, H.; Pan, F.; Jiang, Z.; Cheng, Q. Enhanced Anti-Swelling Property and Dehumidification Performance by Sodium Alginate-Poly(Vinyl Alcohol)/Polysulfone Composite Hollow Fiber Membranes. *J. Membr. Sci.* **2012**, *407−408*, 211−220.
(11) Sousa, F.; Cruz, A.; Fonte, P.; Pinto, I. M.; Neves-Petersen, M. T.; Sarmento, B. A New Paradigm for Antiangiogenic Therapy through Controlled Release of Bevacizumab from Plga Nanoparticles. *Sci. Rep.* **2017**, *7*, 3736.
(12) Long, E.; Lin, H.; Liu, Z.; Wu, X.; Wang, L.; Jiang, J.; An, Y.; Lin, Z.; Li, X.; Chen, J. An Artificial Intelligence Platform for the Multihospital Collaborative Management of Congenital Cataracts. *Nat. Biomed. Eng.* **2017**, *1*, 0024.
(13) Liu, K.; Dong, L.; Xu, Y.; Yan, X.; Li, F.; Lu, Y.; Tao, W.; Peng, H.; Wu, Y.; Su, Y. Stable Gadolinium Based Nanoscale Lyophilized Injection for Enhanced Mr Angiography with Efficient Renal Clearance. *Biomaterials* **2018**, *158*, 74−85.
(14) Leventis, H. C.; King, S. P.; Sudlow, A.; Hill, M. S.; Molloy, K. C.; Haque, S. A. Nanostructured Hybrid Polymer-Inorganic Solar Cell Active Layers Formed by Controllable in Situ Growth of Semiconducting Sulfide Networks. *Nano Lett.* **2010**, *10*, 1253−1258.
(15) Zeng, Q.; Chen, Z.; Liu, F.; Jin, G.; Du, X.; Ji, T.; Zhao, Y.; Yue, Y.; Wang, H.; Meng, D. Aqueous-Processed Polymer/Nanocrystals Hybrid Solar Cells: The Effects of Chlorine on the Synthesis of Cdte Nanocrystals, Crystal Growth, Defect Passivation, Photocarrier Dynamics, and Device Performance. *Sol. RRL* **2017**, *1*, 1600020.
(16) Li, X.; Gao, J.; Xue, L.; Han, Y. Porous Polymer Films with Gradient-Refractive-Index Structure for Broadband and Omnidirectional Antireflection Coatings. *Adv. Funct. Mater.* **2010**, *20*, 259−265.
(17) Fukada, K.; Shiratori, S. Gradient Functional Characteristic of Polymer/Nanoparticle Stacks on a Polyethylene Naphthalate Film. *Ind. Eng. Chem. Res.* **2015**, *54*, 979−986.
(18) Fang, C.-Y.; Liu, Y.-L.; Lee, Y.-C.; Chen, H.-L.; Wan, D.-H.; Yu, C.-C. Nanoparticle Stacks with Graded Refractive Indices Enhance the Omnidirectional Light Harvesting of Solar Cells and the Light Extraction of Light-Emitting Diodes. *Adv. Funct. Mater.* **2013**, *23*, 1412−1421.
(19) Jasieniak, J.; Pacifico, J.; Signorini, R.; Chiasera, A.; Ferrari, M.; Martucci, A.; Mulvaney, P. Luminescence and Amplified Stimulated Emission in CdS-ZnS-Nanocrystal-Doped TiO_2 and ZrO_2 Waveguides. *Adv. Funct. Mater.* **2007**, *17*, 1654−1662.
(20) Sohn, I.-S.; Park, C.-W. Novel Method for the Fabrication of Gradient-Index Plastic Optical Fibers. *AIChE J.* **2003**, *49*, 2499−2509.
(21) Song, D.-P.; Li, C.; Li, W.; Watkins, J. J. Block Copolymer Nanocomposites with High Refractive Index Contrast for One-Step Photonics. *ACS Nano* **2016**, *10*, 1216−1223.
(22) Mao, X.; Lin, S.-C. S.; Lapsley, M. I.; Shi, J.; Juluri, B. K.; Huang, T. J. Tunable Liquid Gradient Refractive Index (L-GRIN) Lens with Two Degrees of Freedom. *Lab Chip* **2009**, *9*, 2050−2058.
(23) Kim, D. C.; Dunn, R. C. Integrating Whispering Gallery Mode Refractive Index Sensing with Capillary Electrophoresis Separations Using Phase Sensitive Detection. *Anal. Chem.* **2015**, *88*, 1426−1433.
(24) Tsai, C.-L.; Liou, G.-S. Highly Transparent and Flexible Polyimide/ZrO2 Nanocomposite Optical Films with a Tunable Refractive Index and Abbe Number. *Chem. Commun.* **2015**, *51*, 13523−13526.
(25) Lü, C.; Yang, B. High Refractive Index Organic-Inorganic Nanocomposites: Design, Synthesis and Application. *J. Mater. Chem.* **2009**, *19*, 2884−2901.
(26) Lü, C.; Guan, C.; Liu, Y.; Cheng, Y.; Yang, B. PbS/Polymer Nanocomposite Optical Materials with High Refractive Index. *Chem. Mater.* **2005**, *17*, 2448−2454.
(27) Kyprianidou-Leodidou, T.; Althaus, H.-J.; Wyser, Y.; Vetter, D.; Büchler, M.; Caseri, W.; Suter, U. W. High Refractive Index Materials of Iron Sulfides and Poly(ethylene oxide). *J. Mater. Res.* **1997**, *12*, 2198−2206.
(28) Antonello, A.; Brusatin, G.; Guglielmi, M.; Martucci, A.; Bello, V.; Mattei, G.; Mazzoldi, P.; Pellegrini, G. Hybrid Organic-Inorganic ZnS-Loaded Nanocomposite Films for Stable Optical Coatings. *Thin Solid Films* **2010**, *518*, 6781−6786.
(29) Lü, C.; Cui, Z.; Wang, Y.; Li, Z.; Guan, C.; Yang, B.; Shen, J. Preparation and Characterization of ZnS-Polymer Nanocomposite Films with High Refractive Index. *J. Mater. Chem.* **2003**, *13*, 2189−2195.
(30) Sergienko, N.; Godovsky, D.; Zavin, B.; Lee, M.; Ko, M. Nanocomposites of ZnS and Poly-(dimethyl)-block-(phenyl)siloxane as a New High-Refractive-Index Polymer Media. *Nanoscale Res. Lett.* **2012**, *7*, 181.
(31) Lee, L.-H.; Chen, W.-C. High-Refractive-Index Thin Films Prepared from Trialkoxysilane-Capped Poly(methyl methacrylate)-Titania Materials. *Chem. Mater.* **2001**, *13*, 1137−1142.
(32) Liu, B.-T.; Li, P.-S. Preparation and Characterization of High-Refractive-Index Polymer/Inorganic Hybrid Films Containing TiO_2 Nanoparticles Prepared by 4-Aminobenzoic Acid. *Surf. Coat. Technol.* **2013**, *231*, 301−306.
(33) Lee, S.; Shin, H.-J.; Yoon, S.-M.; Yi, D. K.; Choi, J.-Y.; Paik, U. Refractive Index Engineering of Transparent ZrO_2-Polydimethyldiloxane Nanocomposites. *J. Mater. Chem.* **2008**, *18*, 1751.
(34) Kudo, S.; Nagase, K.; Kubo, S.; Sugihara, O.; Nakagawa, M. Optically Transparent and Refractive Index-Tunable ZrO_2/Photopolymer Composites Designed for Ultraviolet Nanoimprinting. *Jpn. J. Appl. Phys.* **2011**, *50*, 06GK12.
(35) Liu, H.-T.; Zeng, X.-F.; Zhao, H.; Chen, J.-F. Highly Transparent and Multifunctional Polymer Nanohybrid Film with Superhigh ZnO Content Synthesized by a Bulk Polymerization Method. *Ind. Eng. Chem. Res.* **2012**, *51*, 6753−6759.
(36) Tan, S. T.; Chen, B. J.; Sun, X. W.; Fan, W. J.; Kwok, H. S.; Zhang, X. H.; Chua, S. J. Blueshift of Optical Band Gap in ZnO Thin Films Grown by Metal-Organic Chemical-Vapor Deposition. *J. Appl. Phys.* **2005**, *98*, 013505.
(37) Zhou, S.; Wu, L. Phase Separation and Properties of UV-Curable Polyurethane/Zirconia Nanocomposite Coatings. *Macromol. Chem. Phys.* **2008**, *209*, 1170−1181.
(38) Luo, K.; Zhou, S.; Wu, L.; Gu, G. Dispersion and Functionalization of Nonaqueous Synthesized Zirconia Nanocrystals via Attachment of Silane Coupling Agents. *Langmuir* **2008**, *24*, 11497−11505.
(39) Neto, P. D. L.; Atik, M.; Avaca, L. A.; Aegerter, M. A. Sol-Gel ZrO_2 Coating for Chemical Protection of Stainless Steel. *J. Sol-Gel Sci. Technol.* **1994**, *1*, 177−184.
(40) Xu, X.; Wang, X. Fine Tuning of the Sizes and Phases of ZrO_2 Nanocrystals. *Nano Res.* **2009**, *2*, 891.
(41) Li, W.; Huang, H.; Li, H.; Zhang, W.; Liu, H. Facile Synthesis of Pure Monoclinic and Tetragonal Zirconia Nanoparticles and Their Phase Effects on the Behavior of Supported Molybdena Catalysts for Methanol-Selective Oxidation. *Langmuir* **2008**, *24*, 8358−8366.
(42) Zhao, N.; Pan, D.; Nie, W.; Ji, X. Two-Phase Synthesis of Shape-Controlled Colloidal Zirconia Nanocrystals and Their Characterization. *J. Am. Chem. Soc.* **2006**, *128*, 10118−10124.
(43) Joo, J.; Yu, T.; Kim, Y. W.; Park, H. M.; Wu, F.; Zhang, J. Z.; Hyeon, T. Multigram Scale Synthesis and Characterization of Monodisperse Tetragonal Zirconia Nanocrystals. *J. Am. Chem. Soc.* **2003**, *125*, 6553−6557.
(44) Zhou, S.; Garnweitner, G.; Niederberger, M.; Antonietti, M. Dispersion Behavior of Zirconia Nanocrystals and Their Surface Functionalization with Vinyl Group-Containing Ligands. *Langmuir* **2007**, *23*, 9178−9187.
(45) Wang, X.; Li, Y. Monodisperse Nanocrystals: General Synthesis, Assembly, and Their Applications. *Chem. Commun.* **2007**, *28*, 2901−2910.

DOI: 10.1021/acs.langmuir.8b00160
Langmuir 2018, 34, 6806−6813

(46) Singhal, A.; Toth, L. M.; Lin, J. S.; Affholter, K. Zirconium(IV) Tetramer/Octamer Hydrolysis Equilibrium in Aqueous Hydrochloric Acid Solution. *J. Am. Chem. Soc.* **1996**, *118*, 11529−11534.
(47) Chung, P.-T.; Chiou, S.-H.; Tseng, C.-Y.; Chiang, A. S.-T. The Preparation and Evaluation of a Zirconia/Oligosiloxane Nanocomposite for LED Encapsulation. *ACS Appl. Mater. Interfaces* **2016**, *8*, 9986−9993.
(48) Scagliotti, M.; Parmigiani, F.; Samoggia, G.; Lanzi, G.; Richon, D. Structural Properties of Plasma-Sprayed Zirconia-Based Electrolytes. *J. Mater. Sci.* **1988**, *23*, 3764−3770.
(49) Kontoyannis, C. G.; Orkoula, M. Quantitative Determination of the Cubic, Tetragonal and Monoclinic Phases in Partially Stabilized Zirconias by Raman Spectroscopy. *J. Mater. Sci.* **1994**, *29*, 5316−5320.
(50) Guo, G. Y.; Chen, Y. L. New Zirconium Hydroxide. *J. Mater. Sci.* **2004**, *39*, 4039−4043.
(51) Liu, C.; Hajagos, T. J.; Chen, D.; Chen, Y.; Kishpaugh, D.; Pei, Q. Efficient One-Pot Synthesis of Colloidal Zirconium Oxide Nanoparticles for High-Refractive-Index Nanocomposites. *ACS Appl. Mater. Interfaces* **2016**, *8*, 4795−4802.
(52) Chang, H.-M.; Liao, C. A Parallel Derivation to the Maxwell-Garnett Formula for the Magnetic Permeability of Mixed Materials. *Condens. Matter Phys.* **2011**, *01*, 55−58.
(53) Aspnes, D. E. Local-Field Effects and Effective-Medium Theory: A Microscopic Perspective. *Am. J. Phys.* **1982**, *50*, 704−709.

DOI: 10.1021/acs.langmuir.8b00160
Langmuir 2018, 34, 6806−6813